Autonomous Construction of Lunar Landing Pad Infrastructure Using In-Situ Resource Utilization and Microwave Sintering

Eider Belda Cano*, Jonah Bradley*, Ty Brennan*, Timothy Currey*, Katherine Evans*, Duncan Foster*, Nicholas Harvey*, Robert Higinbotham*, Abinav Khadka*, Braeden Peterson*, and Hugh Young III*
Virginia Polytechnic Institute and State University, Blacksburg, VA 24061

Repeated launch and landing operations on the lunar surface pose a significant risk to infrastructure due to high-velocity plume ejecta from loose lunar regolith. To address this hazard, VT LUNA has designed an autonomous payload for delivery aboard Astrobotic's Griffin lunar lander that constructs hexagonal landing pad tiles using In-Situ Resource Utilization (ISRU) and microwave sintering. The system consists of a small collection rover and a stationary tile-manufacturing unit, together requiring less than 200 kg of delivered mass. A physics-based sintering model was developed to determine the optimal microwave applicator area, operating at MHz and 4 kW, resulting in a complete tile in approximately hours per the power budget. Sintered regolith tiles are shown to meet the 423.99 kPa impact requirement of a 50,000 kg Human Landing System. The design prioritizes scalability, enabling incremental expansion of landing pad infrastructure in support of NASA's Artemis program.

I. Nomenclature

A_a	=	microwave applicator area, m^2
A_t	=	tile face area, m^2
CP	=	specific heat capacity, $J\,kg^{-1}\,K^{-1}$
E	=	electric field strength, $V\,m^{-1}$
f	=	microwave frequency, Hz
h	=	tile thickness, m
h_L	=	sintering layer thickness, m
J	=	total energy required, kW h
k'	=	dielectric constant
K	=	equation constant, $F\,m^{-1}$
n_L	=	number of sintering layers
P	=	volumetric power density, $W\,m^{-3}$
P_s	=	system power draw, W
t	=	sintering time, s
T_0	=	initial temperature, °C
T_t	=	target sintering temperature, °C
ΔT	=	heating rate, $°C\,s^{-1}$
η	=	microwave system efficiency
ρ	=	regolith bulk density, $kg\,m^{-3}$
$\tan\delta$	=	loss tangent
ε_0	=	permittivity of free space, $F\,m^{-1}$
CONOPS	=	Concept of Operations
GNC	=	Guidance, Navigation, and Control
HLS	=	Human Landing System
IMU	=	Inertial Measurement Unit
ISRU	=	In-Situ Resource Utilization
MLI	=	Multi-Layer Insulation
PSR	=	Permanently Shadowed Region

*Undergraduate Student, Dept. of Aerospace and Ocean Engineering, Virginia Tech.

RF = Radio Frequency
VSD = Value System Design
WLAN = Wireless Local Area Network

II. Introduction

THE NASA's Artemis program is spearheading the effort to bring humanity back to the moon, this time to establish a permanent foothold and create a sustainable, lasting human presence on the lunar surface.

Artemis III plans to deliver astronauts to the lunar surface. This will be the first crewed lunar landing since 1972, targeting exploration of the lunar South Pole region. This mission moves beyond orbital operations to surface access by integrating NASA's Orion spacecraft with a commercial Human Landing System (HLS), currently being developed with SpaceX's Starship variant. The mission emphasizes scientific investigation of polar geology, volatiles, like water and ice, and surface processes that are critical for understanding the Moon's history and supporting future long-duration missions. Artemis III will also test advanced spacesuits and surface mobility concepts. Artemis IV is the first mission planned to interact with NASA's "Gateway", a small lunar orbiting outpost being built in partnership with international space agencies. Scheduled for September of 2028, Artemis IV will deliver the Lunar I-Hab module to Gateway and support additional lunar surface visits. This mission begins the creation of a sustained lunar orbital infrastructure, improving access, flexibility, and science return for surface missions while serving as a testbed for technologies needed for Mars exploration. During these missions, most notably Artemis III and IV, a crew will be deployed, exploring the south pole region of the moon and debuting the first lunar space station. To achieve this level of sustained presence on the harsh environment that is the lunar surface, extensive infrastructure is required. This is where COSMIC and its challenge steps in.

In 2022, the White House released a national strategy for the advancement of In-Space Assembly and Manufacturing (ISAM) capabilities. The strategy outlined six general steps to advance and prioritize ISAM development. As a response, the Consortium for Space Mobility and ISAM Capabilities (COSMIC) was created. COSMIC acts as a hub for over 250 organizations, including but not limited to: federal agencies, universities, research institutes, and commercial companies, to assess ISAM needs and advance its prerogative. In their newest challenge, the C3 COSMIC Capstone Challenge, COSMIC invites students to develop conceptual missions and designs for spacecraft operations in-orbit or on the lunar surface.

The VT LUNA team has elected to participate in Track 2 of this capstone challenge: C3-Lunar, with problem statement as follows: Design a payload, to be delivered by the Griffin lunar lander, that can create infrastructure for a permanent lunar outpost.

Given this challenge, the goal of VT LUNA is to design an autonomous system capable of constructing lunar infrastructure, specifically lunar landing pad tiles, using In-Situ Resource Utilization (ISRU) techniques. The mission timeline targets a launch in the late 2020s or early 2030s, aligning with the Artemis program support window.

III. Mission Architecture

A. Mission Objectives and Requirements

The mission is intended to demonstrate a practical In-Situ Resource Utilization (ISRU) capability that supports future lunar surface infrastructure. Its primary objective is to autonomously manufacture durable landing pad tiles from lunar regolith after delivery aboard the Griffin lunar lander. In doing so, the system addresses one of the main hazards associated with repeated lunar landings: high-velocity plume ejecta that can damage nearby surface assets and compromise long-term surface operations [1]. Beyond tile production itself, the mission must also validate autonomous surface operations, regolith handling, and survival in the lunar environment under strict lander resource constraints.

The design is driven primarily by mass and power limitations. Because the payload must fit within the Griffin lander allocation, the complete system is constrained to a total mass below 200 kg and must remain within a limited fraction of the available payload volume. These restrictions strongly influence subsystem sizing, material selection, and the decision to separate the architecture into a lightweight collection rover and a stationary tile-manufacturing unit. Power is similarly restrictive: the system must complete excavation, transfer, and microwave sintering operations within the peak power available from the lander and within an energy budget that makes tile production practical over the mission lifetime [2][3].

Table 2 Condensed mission requirements for the lunar tile-manufacturing payload [2]

Condensed System Requirements	
SYS1.0	The integrated system shall have a total mass of less than 200 kg and remain within the allocated Griffin payload volume.
SYS2.0	The system shall collect, accept, and process lunar regolith as the primary feedstock for tile production.
SYS3.0	The system shall autonomously manufacture structural tiles using ISRU methods without requiring consumable binder material delivered from Earth.
SYS4.0	The system shall produce hexagonal tiles that meet the required structural and thermal performance criteria for landing pad applications.
SYS5.0	The system shall operate autonomously on the lunar surface, including health monitoring, fault response, and completion of nominal production activities.
SYS6.0	The system shall survive and function within the lunar surface environment while operating within the allocated peak power and energy-per-tile budget.

These condensed requirements capture the primary mission drivers while omitting secondary performance goals. In particular, the architecture is shaped by two dominant constraints: limited delivered mass and limited available power. Together, these constraints motivate a compact, highly autonomous system that minimizes mobility burden, keeps energy-intensive processing stationary, and uses lunar regolith directly as the construction material in support of scalable lunar infrastructure development [**?**].

B. Concept of Operations

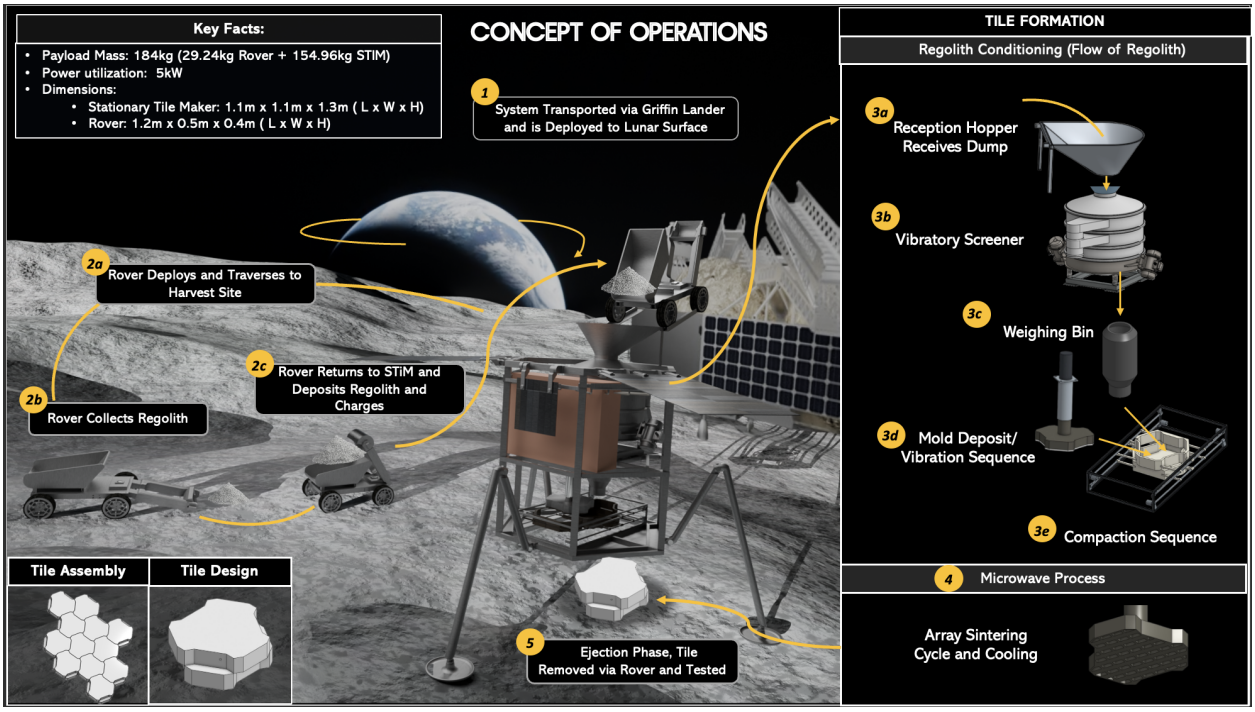

Fig. 1 Concept of Operations for the mission.

The mission employs the Griffin Lander to deliver the payload to the lunar surface. Following landing, the system transitions to autonomous surface operations and executes a cyclical operational process designed to collect lunar regolith, process it on-site, and fabricate solid tiles for surface infrastructure applications. An overview of the operational

sequence is shown in Figure 1. The concept of operations proceeds as follows:

1) **Deployment and Initialization:** After landing, the lander performs system health checks and initializes surface operations. Solar arrays deploy to provide power, and the stationary tile-fabrication system is deployed from the lower deck of the Griffin Lander to the lunar surface.
2) **Regolith Collection:** A small rover deploys from the lander and traverses to a designated harvesting area, where loose lunar regolith is collected using an excavator arm.
3) **Material Transfer and Recharging:** Once loaded, the rover returns to the stationary tile-fabrication unit, docks, and transfers the collected regolith into a hopper via a ramp or elevator mechanism. During docking, the rover connects to a wireless charging node integrated into the lander to recharge its battery.
4) **Regolith Processing:** Inside the fabrication unit, the regolith is sifted using a vibratory screen to remove oversized particles. The processed material is then weighed and distributed into a mold to ensure consistent tile geometry.
5) **Sintering:** A microwave laser system melts and sinters the regolith into a solid tile.
6) **Cooling & Release:** The fabricated tile undergoes controlled cooling to mitigate thermal stresses and prevent cracking. Once cooled, the tile is released onto the lunar surface.

This cycle is repeated throughout the mission, enabling gradual production of surface tiles as the rover alternates between regolith collection and battery recharging. By keeping the primary processing equipment stationary and assigning mobility to the rover, the system maintains operational simplicity while supporting scalable construction of landing pad infrastructure.

C. Fabrication Method Trade Study

To select a tile fabrication approach compatible with the mission mass and power constraints, VT LUNA compared binder-based construction, solar sintering, and microwave sintering. Binder-based methods were eliminated early because they require Earth-delivered consumables, which reduce scalability and consume too much of the 200 kg mass budget [4]. The final trade therefore focused on the two sintering approaches, with microwave sintering emerging as the preferred option because of its operational flexibility, controllability, and compatibility with the rest of the payload architecture [5].

Table 3 Fabrication method trade study.

Weights →	**0.30**	**0.20**	**0.25**	**0.25**	**1.00**
Technology	**Mass Score**	**Power Score**	**Scale Score**	**Effect. Score**	**Total Score**
Microwave Sintering	0.37	0.05	0.45	0.36	**0.324**
Solar Sintering	0.19	0.42	0.20	0.12	**0.221**
Binder-Based	0.05	0.42	0.10	0.28	**0.194**
Heating Plates	0.24	0.03	0.15	0.16	**0.156**
Pressed Brick	0.15	0.08	0.10	0.08	**0.105**

Microwave sintering was selected because it provides the best balance of mass efficiency, controllability, and mission flexibility. Unlike solar sintering, it does not depend on direct illumination, and unlike binder-based methods, it does not require consumable material transported from Earth [4, 5]. Although it imposes a moderate power demand, it offers the strongest path for scalable tile production over the full mission duration.

D. System Architecture Trade Study

In order to complete the mission objective outlined and use ISRU to create lunar landing tiles, several general architectures were considered during the design process. These architectures fell into the following categories: Independent Rover, Umbilical Cord, Dock to Charge, and Stationary Tile Maker. Each option had its own strengths and weaknesses, and the final design was selected based on how well it balanced mobility, power access, complexity, and scalability.

Table 4 System architecture trade study summary.

Architecture	Pros	Cons	Outcome
Independent Rover	High mobility and range, strong mission heritage, and ability to access a variety of regolith sources	Must carry its own solar arrays and battery system, increasing mass, volume, and limiting high-power construction operations	Rejected as a full architecture because it is better suited for exploration and science missions than energy-intensive construction
Umbilical Cord	Continuous access to lander power and reduced need for a large onboard battery	Tether management introduces risk of abrasion, entanglement, limited mobility, and interference with other surface assets	Rejected because the tether system added too much logistical and operational complexity
Dock to Charge	Allows rover mobility without a tether while still using lander power for recharge and high-power operations	Limited by sortie range, charging downtime, and docking interface complexity	Retained as a useful part of the final concept because it provides a practical solution to rover power draw
Stationary Tile Maker	Simplified mechanical design, continuous access to high lander power, and strong fabrication capability	Cannot relocate to new regolith sources and depends on usable material being available near the lander	Retained as a useful part of the final concept because it is the most effective configuration for tile production

The independent rover architecture had its merits, no doubt, but the mass and, more importantly, the power concerns drove VT LUNA away from using it as the primary design. The umbilical cord architecture solved the rover power issue, but the added complexity and risk from the tether system provided a logistical hurdle that was deemed too difficult to overcome.

With this, VT LUNA selected a hybrid architecture that combines the best aspects of the dock-to-charge and stationary tile maker concepts. In the final design, a lightweight mobile rover is used to collect and transport regolith, while a stationary manufacturing unit mounted to the lander performs the energy-intensive tile fabrication process. This allows the system to maintain mobility where needed while taking full advantage of the lander's available power for manufacturing.

IV. Landing Site Selection and Regolith Characterization

A. Site Selection

The selection of a suitable lunar landing site is critical to mission success, particularly for enabling autonomous construction of infrastructure such as landing pads. The chosen site must balance power availability, terrain safety, communication capability, thermal stability, and regolith suitability.

For this mission, five primary criteria were used in evaluating potential landing locations:

- **Solar Illumination:** High levels of sunlight are required to support continuous power generation. Polar regions are preferred due to their extended periods of illumination, with some areas receiving up to 85–90% annual sunlight [6].
- **Terrain Safety and Accessibility:** The landing site must be relatively flat and free of hazards such as large rocks, craters, or steep slopes to ensure safe landing and rover mobility.
- **Communication Access:** A direct line-of-sight to Earth is necessary for reliable data transmission and command operations.
- **Thermal Stability:** Regions with consistent solar exposure experience reduced temperature extremes, improving system reliability.
- **Regolith Quality:** The surface material must be sufficiently thick and stable to support sintering processes and structural integrity.

The lunar south pole was selected as the general region of interest due to its favorable illumination conditions and proximity to permanently shadowed regions (PSRs), which may contain water ice. These characteristics make it a strong candidate for sustained exploration and infrastructure development. However, the terrain is more rugged than equatorial regions, introducing additional challenges.

When choosing where to land and build on the Moon, sunlight remains one of the most important factors. Illumination varies dramatically across the lunar surface, making the poles particularly valuable for solar energy access. Figure **??** shows the average yearly solar illumination for the lunar south pole at a height of 2 m above the surface. The brightest zones, located around the rim of Shackleton Crater and extending toward de Gerlache Crater and the Connecting Ridge, stay illuminated for as much as 85–90% of the lunar year [6]. This makes them some of the most favorable locations on the Moon for generating continuous solar power.

NASA initially identified 13 candidate landing regions for Artemis missions, later refining the list to 9 sites based on illumination, terrain, and communication constraints [7, 8]. These include areas such as Haworth, Malapert Massif, Mons Mouton Plateau, and the Nobile Rim regions. A key trade-off emerged between illumination and terrain safety. For example, regions near Shackleton Crater offer excellent illumination but feature steep slopes and significant elevation changes, increasing landing risk. As a result, such locations were deemed unsuitable despite their favorable lighting conditions [6].

The selected landing site is located near the Mons Mouton Plateau, specifically within the Nobile Rim 1 region. This site was chosen as it provides the best overall balance across all selection criteria [8]. Mons Mouton Plateau offers approximately 70–80% annual sunlight, which is sufficient for sustained power generation, while also providing relatively smooth and flat terrain that reduces landing and operational risk. The site maintains strong line-of-sight visibility with Earth, is located near multiple permanently shadowed regions including Haworth and de Gerlache, and contains stable regolith suitable for construction using sintering techniques [8].

Although other sites offered higher illumination, they were rejected due to increased risk associated with terrain and accessibility. De Gerlache Rim 2 and Malapert Massif were also considered, but both introduce operational challenges that outweigh their advantages, making them less suitable than the broader and more accessible Mons Mouton Plateau [8].

Overall, landing site selection is driven primarily by safety and operational feasibility, with illumination and resource access serving as secondary but still critical factors. The Mons Mouton Plateau (Nobile Rim 1) provides a balanced solution that supports both immediate mission needs and long-term lunar infrastructure development.

B. Regolith Composition and Sintering Properties

Lunar regolith plays a critical role in the feasibility of in-situ resource utilization (ISRU) and construction processes such as sintering. Its physical and chemical properties vary significantly depending on location, driven by differences in lunar topography and geological history.

1. General Characteristics

The Moon's surface exhibits significant topographical variation, ranging from approximately −8 km to +10 km relative to a reference ellipsoid. These variations correspond to distinct geological regions, including basalt plains, highlands, and high- and low-titanium (Ti) mare regions. As a result, the composition and structure of the regolith differ across the lunar surface.

Lunar regolith is primarily composed of metal oxides, with silicon dioxide (SiO_2) as the dominant constituent. Other major components include aluminum oxide, iron oxide, calcium oxide, and magnesium oxide. These materials strongly influence both mechanical behavior and thermal response [9].

2. Topographical Influence on Regolith

Different lunar regions exhibit distinct regolith characteristics:

- **Basalt Plains:** Formed from ancient lava flows, these regions are relatively flat and rich in iron and titanium. However, their formation leads to variability in regolith consistency due to impact history.
- **Highlands:** Located at higher elevations, particularly near the poles, these areas have different compositions and more rugged terrain.
- **High-Ti Mare:** Rich in titanium dioxide and iron oxide, these regions contain highly uniform, fine, sand-like regolith. They exhibit strong microwave absorption properties, making them ideal for sintering.

- **Low-Ti Mare:** Characterized by lower titanium content and more stable terrain, these regions tend to have larger grain sizes and less loose regolith.

These variations directly impact the suitability of regolith for construction and processing applications [9, 10].

3. Chemical Composition and Effects

The chemical composition of lunar regolith determines its melting behavior and response to energy input. Since the material is primarily composed of metal oxides, it exhibits high dielectric loss, allowing it to efficiently absorb energy during processes such as microwave sintering.

Key observations include:

- Iron oxide (FeO) and titanium dioxide (TiO_2) significantly enhance energy absorption.
- Silicon dioxide provides structural stability but is less reactive during heating.
- Variations in composition across locations lead to different optimal processing temperatures and methods.

Because of this variability, the exact sintering conditions depend on the selected landing site [9, 10].

4. Particle Size and Density

Particle size distribution is a critical factor in regolith processing. Studies show that an average grain size of less than 600 μm is optimal for sintering applications. At this scale:

- Particles pack more efficiently, increasing density
- Molten material can flow into gaps, improving structural integrity
- The final product exhibits fewer voids and higher strength

If the particle size is too large, gaps form between molten regions during sintering, preventing the formation of a cohesive structure [11].

5. Thermal and Mechanical Behavior

Lunar regolith exhibits several important thermal and mechanical properties:

- High thermal stability due to silicon dioxide content
- Low thermal expansion, reducing cracking under temperature changes
- High compressive strength when properly sintered

However, the presence of impurities and variations in composition can weaken the final material. A more homogeneous composition results in stronger, more reliable structures [9].

6. Implications for Sintering

The properties of lunar regolith strongly influence the effectiveness of sintering processes:

- High iron and titanium content improves microwave absorption and heating efficiency
- Fine, uniform particles enable consistent layer formation
- Controlled temperature profiles are required to prevent shrinkage, porosity, and material degradation

Excessive heating can lead to mass loss, gas release, and pore formation, weakening the final structure. Therefore, sintering must be carefully controlled to maintain material integrity [12].

7. Summary

Overall, lunar regolith is a highly variable but valuable construction material. Its effectiveness depends on composition, particle size, and thermal behavior. Regions with high titanium and iron content, combined with fine particle sizes, provide the most favorable conditions for sintering and infrastructure development.

V. System Design

A. Design Properties

The design constraints of the tile design are largely determined by the tile manufacturing process, which imposes unique constraints due to the characteristics of microwave sintering and of the specific tile maker's design, resulting in RTR 2.0. The aforementioned radial shrinkage of the tiles by approximately 6.17% during the cooling process imposes

additional constraints on tile design [13]. As the tiles will shrink inwards horizontally, any internal angles of the mold would therefore be put under pressure by these shrinking tiles, which would result in damage to either the mold or the tile. Therefore, the tiles shall not have internal angles resulting in RTR 2.2.

As there is only one tile maker with a singular mold, only one tile design will be able to be produced. Therefore, the tile produced should be capable of independently forming a solid surface, so the tile shall be a geometry that tesselates, resulting in RTR 2.3.

1. Our Tile Design

Based upon these requirements, the tile design is a modified duel layer hexagon with a circumscribed radius of 0.15 m, and a depth of 0.106 m

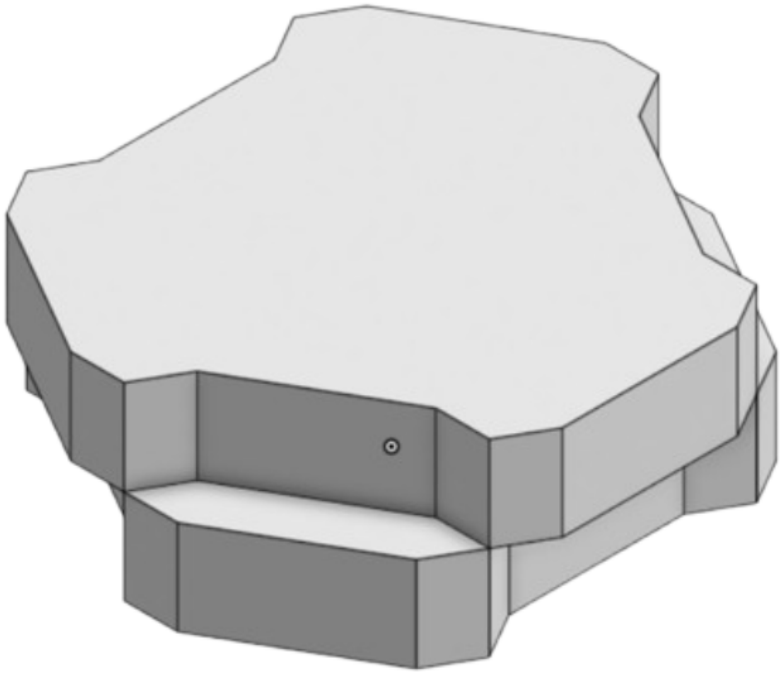

Fig. 2 Image of the tile design, a modified duel hexagon with a circumscribed radius of 0.15 m, a depth of 0.106 m. The double layer allows for simple interlocking of tiles.

This design fulfills RTR 1.0 as it can withstand the 423.99 kPa impact outlined in RTR 1.2 as calculated in equation $t = \sqrt{\frac{K\, p_{max}\, \pi r^2}{\sigma_{\text{bending}}}} * safetyfactor$[14] with K being .398 and the safety factor being 2.3 which is the maximum expected load and therefore fulfills RTR 1.1 and RTR 1.4 as well as their lesser loading conditions. This design also fulfills RTR 1.3 as it's surface area is approximately the same as the tiles used in a research paper where thermal analysis was conducted showing that sintered regolith tiles are capable of withstanding intense heating. [15].

B. Regolith Tile Properties

The requirements for the regolith tiles are derived from two main constraints: the material properties to withstand the applied loads that occur during a launch or landing from a targeted 50,000 kg Human Landing System (HLS); and the manufacturing constraints of the stationary tile maker. To meet the goals of the project, the following requirements were created.

Table 5 Regolith Tile Requirements: This table displays the requirements of the regolith tiles.

Regolith Tile Requirements (RTR)	
RTR 1.0	The tile must survive the landing of a 50,000 kg Human Landing System (HLS).
RTR 1.1	The tiles shall be able to withstand a sustained vertical pressure of 35.4 kPa from the HLS landing plume.
RTR 1.2	The tiles shall withstand 423.99 kPa impact of HLS landing.
RTR 1.3	The tiles shall withstand 17786.3 kW/m^2 heating from the plume of HLS landing.
RTR 1.4	The tiles shall withstand 25.78 kPa static pressure of HLS after landing.
RTR 2.0	The tiles shall be able to be manufactured utilizing the stationary tile maker and the microwave sintering process with no post-processing.
RTR 2.1	The tiles shall be vertically homogeneous.
RTR 2.2	The tiles shall not have internal angles.
RTR 2.3	The tiles shall be a geometry that tessellates.

A 50,000 kg HLS vehicle was chosen, however further research into larger HLS vehicles such as the approximately 100,000 kg SpaceX Starship, should be conducted once these companies have finalized designs and released technical specifications for their systems [16].

C. Material Properties

To determine the necessary strength of the tiles, previous research was assessed in which a Finite Element Analysis (FEA) study simulating a landing of a 50,000 kg HLS was conducted [17].

Table 6 Loading Conditions Experienced by Landing Pad During a Simulated Landing [17].

Timestamp (s)	Max Plume Vertical Pressure (kPa)	Max Plume Heat Flux (kW/m^2)	Leg Stress (kPa)
0	0.00	0.00	0.00
1	8.85	4,446.58	0.00
2	17.70	8,893.15	0.00
3	26.55	13,339.73	0.00
4	35.40	17,786.30	0.00
5 (impact)	0.00	0.00	423.99 (one leg)
6 (static)	0.00	0.00	25.78 (four legs)

From this data the material requirements of the tile were determined (RTR 1.1-1.4). However, research into the strength of sintered tiles shows results that vary widely depending on the types of regolith used and the exact process used to sinter the regolith. Therefore, to fulfill these requirements, it was necessary to isolate and examine the properties that affect tile strength and determine the optimal characteristics for the tile fabrication process. The primary properties that affect the strength of the tiles are:

1. Porosity

The porosity of the tile has been shown to have an extreme effect on the compressive strength of the tiles. An increase in porosity by 10% can cut the compressive strength and failure load in half. [18] A major cause of porosity in the tiles is the particle size of the regolith. When sifted to a particle size below 212 μm the average porosity should be $\approx$ 1.44%.

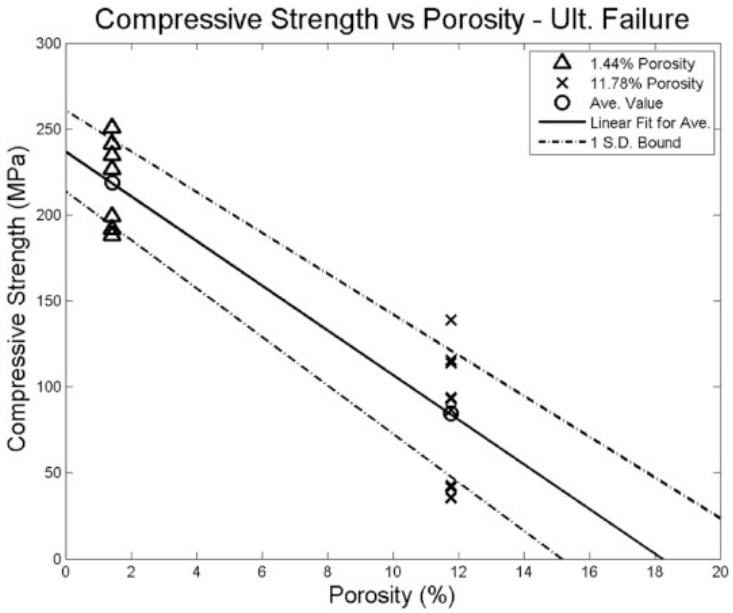

Fig. 3 A graph detailing the relationship between compressive strength and porosity [18].

2. Sintering Temperature and Regolith Composition

Table 7 Material Properties of Sintered Lunar Regolith Simulant Samples by Temperature [13].

1000°C Radial Shrinkage Percentage	0.84%
1000°C Height Shrinkage Percentage	1.16%
1100°C Radial Shrinkage Percentage	1.85%
1100°C Height Shrinkage Percentage	3.15%
1200°C Radial Shrinkage Percentage	6.17%
1200°C Height Shrinkage Percentage	18.13%
1200°C Compression Modulus (MPa)	55.73
1200°C Compressive Strength (MPa)	21.73

Sintering at a temperature higher than the melting point of most or all of the components of the regolith results in a higher compressive strength for the tile. [19] The melting point for these components tends to be below 1200 °C. [20]. Therefore, for this project, the tiles will be sintered at 1200 °C. Sintering at this temperature can allow molten components to fill voids in the tile, slightly increasing density and decreasing porosity.

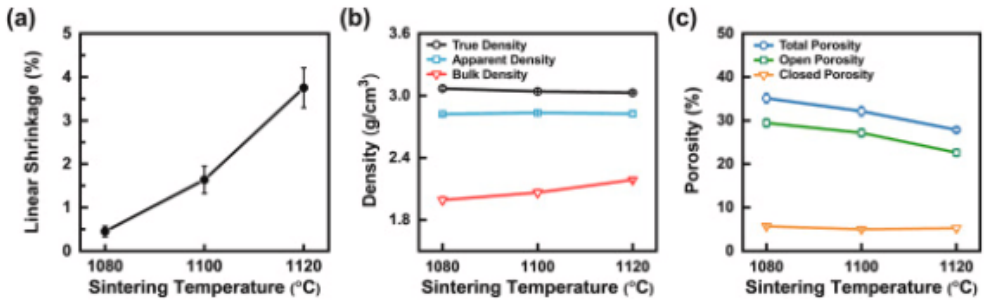

Fig. 4 Graphs with relationships between sintering temperature density, shrinkage, and porosity [19].

However, this does create unique challenges in tile design as this high temperature has a side effect of significantly more material shrinkage as seen in the above table [13]. Due to some components of the regolith evaporating and the molten regolith becoming denser and filling the voids between the particles, the volume of the regolith reduces rather significantly. Sintering regolith from highland or mare regolith can give vastly different results. When sintering highlands regolith, the temperature has to be 50 to 100 °C to achieve the same results as when sintering mare.

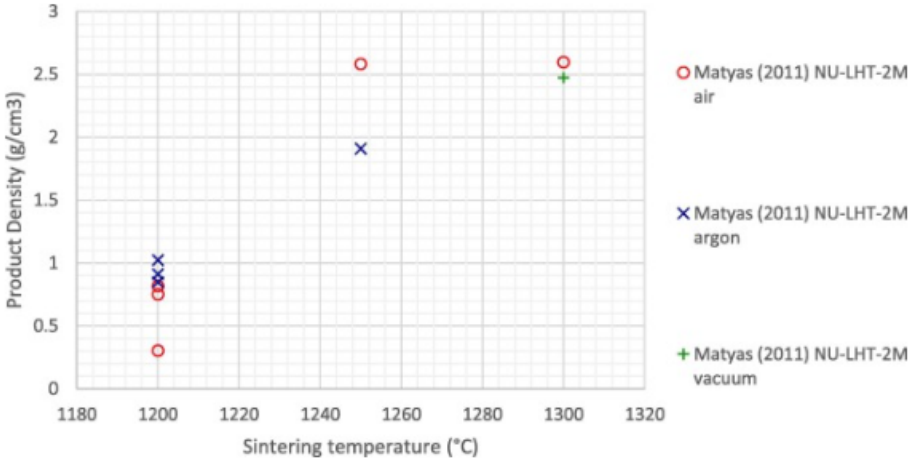

Fig. 5 A graph detailing the relationship between highland sintering temperature and density [20].

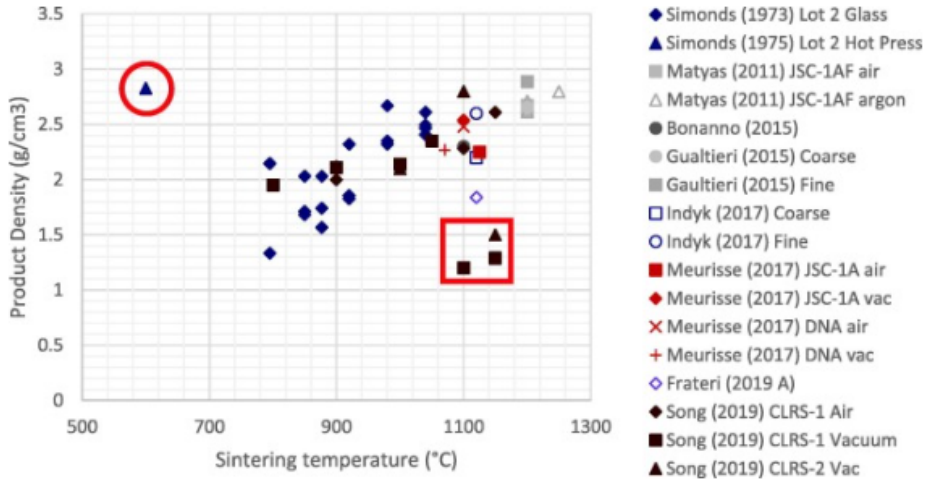

Fig. 6 A graph detailing the relationship between mare sintering temperature and density [20].

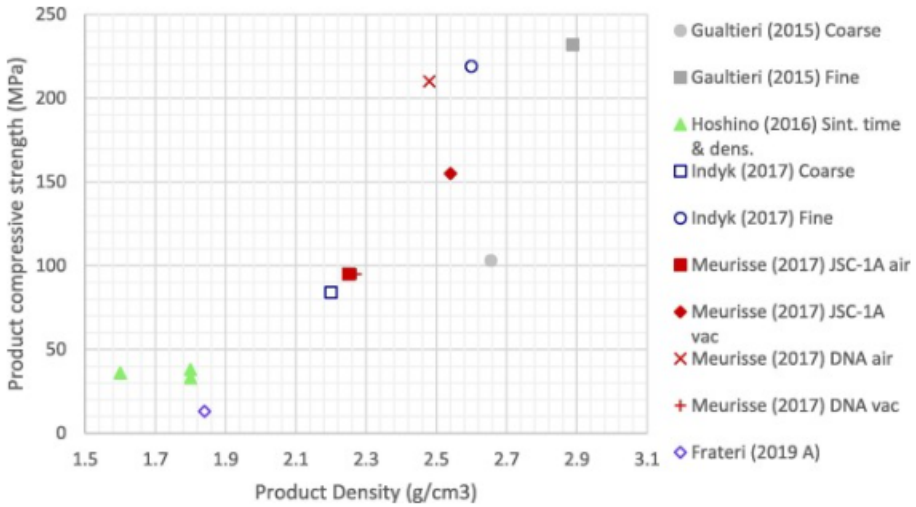

Fig. 7 A graph detailing the relationship between regolith density and compressive strength [20].

The compressive strength of regolith when sintered at 1200 °C can vary [13] greatly when considering the environment that the regolith will be collected from; thus, when determining how to satisfy the minimum requirements for the tiles, the minimum possible properties of th/]kne tiles should be considered. Throughout all the experiments covered by research conducted by VT LUNA, the low end of the compressive strength of the tiles is about 20 MPa. The bending strength tends to be about 28% of the compressive strength[21], so it will be 5.67 MPa. At this compressive strength, the tile will easily withstand the expected compression forces at any reasonable thickness; thus, the tile's thickness should be determined based on its ability to withstand bending stress due to imperfections in the ground supporting it.

D. Microwave Sintering Model

Understanding the required power of all the subsystems is an integral part of ensuring the feasibility of this mission and its architecture. The most power-intensive and complex subsystem is the microwave sinterer. The sinterer must be able to heat 8,268 cm^3 of regolith to 1200 °C. The power required to heat the entire tile simultaneously would exceed the Griffin lander's power output, rendering it impossible. To enable the creation of a tile, sintering will be done in thin layers. Within each layer, about a fifth of it will be sintered at once. With this approach, the instantaneous power draw is low enough to allow the power to be sourced exclusively from the Griffin lander.

Table 8 Core Modeling Equations Required to Relate the Sintering Process to Lunar Regolith Material Properties.[22][23]

Eq.	Expression
(1)	$P = K f E^2 k' \tan(\delta)$
(2)	$\Delta T = \frac{P}{\rho C P}$
(3)	$P_s = \frac{P V}{\eta}$
(4)	$t = \frac{T_t - T_0}{\Delta T}$
(5)	$J = P_s \cdot t$
(6)	$K = K' - jK'' = K_\infty + \frac{K_0 - K_\infty}{1 + (j\omega\tau)^{1-\alpha}}$

1. Method

A model was developed to estimate the power, energy, and time required to sinter a single lunar regolith tile using defined inputs for tile geometry, microwave system characteristics, and material properties. The governing relations for absorbed power and heating rate (Eqs. 1–2)[22] form the foundation of the model and were extended to compute instantaneous power draw, total energy consumption, and total sintering time (Eqs. 3–5). While most parameters are constant or controllable, the dielectric constant and loss tangent of lunar regolith vary strongly with temperature and are critical to accurately capturing system behavior, whereas density and specific heat capacity were assumed constant due to their relatively small variation over the temperature range of interest.

Temperature-dependent dielectric properties were obtained from Apollo-era experimental data[23], which were extracted from published plots using WebPlotDigitizer and fit in MATLAB to generate usable functions with approximately 90% accuracy. With all variables defined, the system reduces to a temperature-dependent differential equation, which was solved numerically using a 1-second time-stepping loop that updates temperature, absorbed power, and cumulative energy until the target sintering temperature is reached. Because available data only extends to 500 °C, values beyond this range were linearly extrapolated.

To determine the most efficient system configuration, a second iteration of the model swept across possible applicator areas, recalculating electric field strength and total sintering time for each case. This captures the inverse relationship between applicator area and field strength and allows identification of the configuration that minimizes total processing time while maintaining sufficient heating, with additional consideration of heat dissipation to ensure the target temperature is achievable.

2. Results

For a hexagonal tile with a face area of 0.0585 m^2 and a depth of 0.106 m, using a layer thickness of 1 mm, the optimized configuration at the full system power of 4 kW resulted in the applicator area expanding to the entire tile surface. This eliminates the need for multiple passes per layer and maximizes energy delivery efficiency. Under these conditions, the model predicts a processing time of approximately 234 seconds per layer, resulting in a total sintering time of 6.9 hours per tile.

These results demonstrate that at higher available power, full-area sintering becomes optimal, significantly reducing total processing time and system complexity. The model also highlights the scalability of the approach, as increased power or parallel systems would further reduce construction timelines, supporting feasibility for larger-scale lunar infrastructure deployment.

E. Regolith Collection Rover

The collection system relies on a small autonomous rover designed to retrieve regolith and transport it to the stationary processing plant. The rover operates in a continuous loop, and there will be four major steps to this process.

The first step is the deployment; the rover will leave the dock/Griffin lander in search of regolith. The navigation system will be initialized as soon as the rover deploys to guide the rover to the best location to retrieve the regolith. The navigation system chosen consists of Wheel Odometry and IMU, which will be used for obstacle detection and alignment. The rover will only be traveling short distances, between the collection site and the lander, which is why this navigation system was chosen. It is lightweight and provides sufficient accuracy while consuming low amounts of power compared to other navigation methods. The tires of the rover were also chosen with the location in mind. Rigid aluminum wheels with grousers are the tires chosen, because the landing site will have loose lunar soil. This type of tires will ensure traction and allow the rover to travel between operational locations.

The second step is collecting the regolith. Once the rover reaches the excavation area, it will begin the collection process. This will be done via a two-joint robotic arm, consisting of a elbow pitch joint and wrist tilt joint. These joints will supply , 8–10 Newton-metre, and 2–3 Newton-metre of torque, respectively, which will allow the arm to scoop loose regolith and transfer it to the hopper. The hopper will be constructed of aluminum alloy, similar to the two-joint robotic arm. The hopper will hold 16 kilograms of regolith, but the rover will return to the stationary tile maker when there are 14.5 kilograms of regolith stored. This accounts for regolith spillage in the rough terrain. The arm will have to have multiple scoops per trip, because the scoop can only hold up to 3 kilograms of regolith at a time.

The third step in the rover cycle is the return to the stationary tile maker. The path will be short and repeatable, which will allow the rover's navigation to be as accurate as possible. Once the rover reaches the stationary tile maker, it will align itself with a telescoping ramp. The ramp will be designed to guide the rover in the exact position needed to dump the regolith into the stationary tile maker's hopper.

Once the rover is aligned to the ramp, it will travel up to the stationary tile maker's hopper. It will start the dumping procedure, starting with the actuation of the hopper's tilt motor. The hoppers will invert, causing the collected regolith to be released in the reception hopper. After the regolith is received, the material-processing sequence starts, which includes screening, weighing, and ultimately microwave sintering inside the stationary tile maker. While this sequence is taking place, the rover will remove itself from the ramp to begin the next step of the cycle.

The last step is dependent on the stage in the tile making process. The rover will either go into dock-to-charge mode, where it will interface with a charging node integrated into the lander, and the 6S Li-ion Battery Pack ($\tilde{4}$00 Wh, 22.2V, $\tilde{1}$8Ah) [24] will have the energy consumed during the previous cycle replenished, or it will continue to gather regolith. The stationary tile maker can hold enough regolith to create multiple tiles, so depending on the rover's charge level, it could be beneficial to continue to gather regolith. The rover will also run basic diagnostic checks while charging to make sure the rover stays operational. Once the charging is complete, the rover will resume autonomous operations. It's also important to note in the lunar night, the rover will return to the charging node, not to charge, but to enter night mode. This will prevent the damage that could be done to the rover over cold nights.

As the rover will completely detach from the Griffin Lunar Lander, it requires its own communication system. This link allows the rover to receive commands, report health and status, transmit sensor data, and coordinate the regolith-collection workflow in real time — without it, the rover cannot safely navigate or function as an integrated part of the landing-pad construction architecture. A direct Earth link would require a high-gain antenna to bridge the approximately 384,000-mile distance [25], adding significant mass and pointing complexity. Instead, the Griffin lander serves as a relay, enabling the use of low-gain antennas. The lander's onboard 2.4 GHz IEEE 802.11n WLAN modem defines the compatibility requirement for the rover's communication hardware [26]. The rover will use a WGM160P Wi-Fi module to maintain a continuous data link with the lander [27], paired with two 2.4 GHz Pagoda low-gain antennas (0.6–1.3 dBi) mounted on opposite sides of the rover. Their wide coverage pattern eliminates the need for precise antenna pointing, and the dual configuration provides redundancy in the event of damage [28]. Given the rover's short operating range from the lander, the limited distance range of low-gain antennas is not a concern.

All electronics will be protected using multilayer insulation (MLI) consisting of aluminized Kapton, Kapton laminate, Mylar, and aerogel. Aluminized Kapton reflects thermal radiation and remains functional across the full range of lunar surface temperatures [29]. Kapton laminate's low absorptance (under 0.14) and low emittance (under 0.04) help regulate both daytime heating and nighttime heat loss [30]. Aerogel, rated to 1100°C and roughly one-third the mass of conventional insulation materials, provides lightweight thermal conductivity protection [31]. The MLI stack will be 10–20 layers, accumulating to only a few millimeters in thickness [32].

F. Other concepts considered

Many different methods were considered in this design, including a completely Independent Rover. In the independent rover architecture, the construction rover carries its own primary power system and operates autonomously

within the local mission area. Power is typically provided by body-mounted or deployable solar arrays coupled with onboard energy storage (batteries and/or capacitors). The rover is responsible for executing the full construction task cycle—regolith collection, transportation, tile fabrication support, and placement—without requiring a physical tether to the lander during normal operation. This was decided against because the rover must carry solar arrays, and large batteries,increasing mass, volume, and potential failure points.

Another idea that was considered is the Umbilical cord method. In the Umbilical Cord architecture, the rover remains physically tethered to the lander via a power cable during operation. The solar array on the lander hosts the primary power generation system, and the rover draws continuous power through the umbilical. The operation is similar to a high-power tool on a long extension cord. A spool mechanism may manage the tether, or it may be laid on the lunar surface. This was decided against because the tether concept drastically decreases scalability and can interfere with future lunar operations, as additional rovers, landers, or human crews will have to navigate around a web of cables.

G. Summary

As it can be seen each component of the rover was evaluated based on its mass, durability, energy efficiency, and lunar environmental constraints in the component selection process. It was decided that this method of regolith collection was the best options given the constraints of the project. [PLACEHOLDER — rover cycle description + arm/wheel/nav tables]

H. Stationary Tile Manufacturing System

1. Stationary Tile Maker Overview

The Stationary Tile Maker is an autonomous system that converts raw lunar regolith into sintered structural tiles through a continuous process chain consisting of: ramp delivery, reception hopper buffering, vibratory sifting, mass metering, mold compaction, microwave sintering, thermal cooling, and final tile ejection. The system is designed to minimize mechanical complexity while ensuring repeatable material preparation and consistent electromagnetic heating conditions.

2. Collection and Feed System

Regolith is delivered by a rover via a telescoping self-centering ramp into a reception hopper. The hopper provides temporary storage and flow regulation through steep wall angles ($\sim 70^\circ$), conductive surface treatment, and vibratory assistance to mitigate bridging and arching in reduced gravity conditions [33]. A controlled outlet gate regulates discharge into the conditioning subsystem, decoupling delivery timing from downstream processing and ensuring continuous operation.

3. Conditioning

Vibratory Sifter The vibratory sifter performs size classification using a three-stage architecture with progressively finer cutoffs of 2.0 mm, 0.8 mm, and 550 μm. This ensures a final particle size distribution below 600 μm, which is necessary for consistent packing density and microwave absorption behavior [34, 35]. The system is driven by a single brushless DC vibratory motor operating at 50 Hz, providing both sieving excitation and auxiliary flow support across the upstream hopper interface. The multi-stage design reduces clogging risk while maintaining high throughput and mechanical robustness.

Weigh Bin After sifting, regolith enters a load-cell-based weigh bin that meters material to a fixed mass of 13.3 kg per tile. The system uses four load cells to ensure measurement redundancy and uniform load distribution. Material is released through a rotary dispensing gate that meters regolith in discrete increments corresponding to 1 mm layer mass ($\sim$1/106 of total tile mass, approximately 12.55 g per cycle), enabling precise layer-by-layer construction.

Sinter Mold Conditioned regolith is deposited into a stainless steel mold that defines final tile geometry. A vibratory settling mechanism ensures uniform distribution prior to compaction. A motor-driven zirconia ceramic plate then applies compressive force to increase packing density, reduce void fraction, and improve microwave coupling efficiency while maintaining electromagnetic transparency during heating.

4. Microwave Sintering

Microwave sintering is performed using volumetric dielectric heating at 915 MHz. The system operates at a total power of 4 kW, supplied by three RIM091K5-20 1.5 kW GaN RF amplifiers. Energy is delivered through a single waveguide antenna matched to the full tile area, enabling full-layer, one-shot sintering without mechanical scanning or phased-array steering.

This architecture minimizes system complexity and failure points while maximizing coupling efficiency into the regolith layer. The use of a single stationary applicator is enabled by the increased power budget, allowing full-area heating per cycle and eliminating the need for distributed or electronically steered excitation systems.

5. Cooling and Ejection

Following sintering, tiles undergo a two-stage cooling process. Initial cooling occurs through conductive heat transfer into the mold assembly, followed by passive radiative cooling to the lunar environment. This staged approach reduces thermal gradients and minimizes residual stress development. Once cooled to a safe handling temperature, a mechanical ejector system removes the finished tile and resets the mold for the next cycle, enabling continuous production..

I. Thermal Management

In the lunar vacuum, convective cooling is absent; all waste heat must be rejected radiatively to deep space per the Stefan-Boltzmann law. Because the payload produces two thermally distinct heat loads, the thermal control system is divided into two independent loops (Fig. 8).

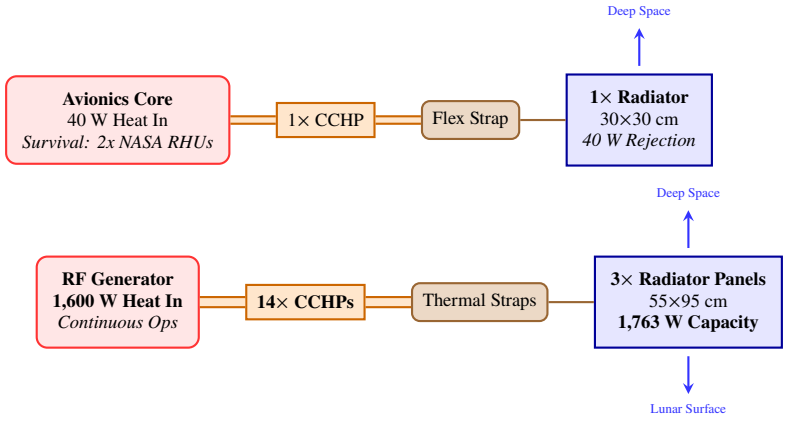

Fig. 8 Hybrid 2-Loop Thermal Architecture Separating Daytime Continuous Ops from Nighttime Survival.

1. Loop 1: Avionics

The rover computer, sensors, and motor controllers produce a continuous 40 W load. A single aluminum-ammonia constant conductance heat pipe (CCHP) transports this heat to a 30×30 cm Al 6061 radiator panel coated with AZ-93 white paint (ε = 0.91, α = 0.14) [36]. A motorized hinge deploys the panel 90° outward during the sunlit phase to face deep space, and stows it flat against the frame during shadow for thermal insulation. During the unpowered 96-hour lunar night, the stowed panel minimizes the parasitic heat leak to 1.6 W. Two NASA Radioisotope Heater Units (RHUs) [37] provide 2 W of continuous internal heat, ensuring the survival core remains safely above its -40°C limit.

2. Loop 2: RF Microwave Generator

The solid-state microwave generator operates at 60% wall-plug-to-RF efficiency [38], producing 1600 W of waste heat at 4 kW input. Because uninterrupted tile production is mission-critical, Phase Change Material (PCM) thermal buffering was discarded in favor of a fully continuous cooling architecture.

Fourteen CCHPs route this heat to three deployable 55×95 cm Al 6061 radiator panels (1.50 m^2 total area, accounting for a 0.06 m^2 frame cutout). These massive arrays reject 1,763 W continuously to deep space and the lunar surface.

Because the 1,600 W waste heat load is fully enveloped by the 1,763 W rejection capacity, the architecture operates with a safe +10.2% thermal margin [39]. This zero-PCM design completely eliminates microwave downtime, allowing 24/7 continuous sintering. During the lunar night, the RF generator is powered off and safely permitted to deep-freeze to -173°C without damage.

Table 9 summarizes the thermal system mass budget.

Table 9 2-Loop Hybrid Thermal Management Mass Budget.

Loop	Component	Mass (kg)
Avionics	Radiator Panel (30×30 cm)	1.36
Avionics	CCHP (×1) + Flex Strap	0.05
Avionics	Motorized Hinge + 2×RHU Pellets	0.48
Avionics Subtotal		**1.89**
Microwave	Radiator Panels (×3, 55×95)	12.26
Microwave	CCHPs (×14) + Flex Straps	1.12
Microwave	Passive Spring Deploy Hinges (×3)	1.50
Microwave Subtotal		**14.88**
Total Thermal System		**16.77**

3. Sintering Chamber Insulation

The sintering chamber is thermally isolated from the cooling loops. Multi-layer insulation (MLI) rated to 1500°C envelops the mold cavity, trapping the 2400 W of RF energy inside the regolith [40, 41]. The only connection between the generator and the chamber is the RF waveguide, which conducts electromagnetic energy but negligible thermal energy. This decoupling ensures that the cooling system removes waste heat from the electronics without diminishing the sintering temperature.

VI. Architecture Analysis

A. Mass Budget

The mass budget was developed using a bottom-up estimation approach based on specific subcomponents identified during the preliminary design phase. This budget separates the mobility platform from the stationary tile maker (STiM), allowing the mass contribution of each system to be evaluated directly.

Table 10 Mass budget summary for the rover and STiM systems.

Rover Mass Budget		STiM Mass Budget	
Component	**Mass (kg)**	**Component**	**Mass (kg)**
Battery Pack	2.80 [24]	Aluminum Frame	41.0
Electronics Components	5.98 [24, 42–45]	3x Support Legs	13.5
Chassis	2.23	Battery Pack	30.0
4x Wheels	1.09	Vibratory Motors	6.35
4x Tires	1.47	Regolith Sifting System	9.69
Bucket	8.16	Cooling System	17.31
2x Scoop Arms	3.87	Hopper & Ramp	5.47
Scoop	3.14	Weigh Bin	5.85
Harness	0.50	Mold System	11.16
Total Mass	**29.24**	Sintering System	9.23
		Total Mass	**154.9**

As shown in Table 10, the rover has a total mass of 29.24 kg, which remains below the 30 kg allocation set at the beginning of the project. The STiM has a total mass of 154.9 kg, bringing the full system mass to 184.14 kg. This keeps the integrated payload within the 200 kg mission limit and leaves a remaining mass margin of 15.86 kg.

The results show that the rover successfully remains lightweight while still carrying the components required for mobility, excavation, sensing, and autonomy. In contrast, the STiM is the primary mass driver of the system due to the structural, power, and processing hardware required for regolith handling and tile fabrication. Overall, the mass budget confirms that the selected architecture is feasible within the mission constraints.

B. Power Budget

The power budget provided by the Griffin lander is 5 kW, as stated in the RFP [2]. The following power budget table gives updated estimates of the total power used by both the rover and the stationary tile factory (STiM) based on the current design. These estimates are based on the selected electronics, components, and expected operating modes of each subsystem, and show that the system remains within the available lander power budget.

Table 11 Power budget summary for the Rover and STiM systems.

Rover Power Budget		
Mode	**Power Draw**	**Description**
Controls	<200 W	Driving, dumping, and communications
Digging/Scoop/Dump	<175 W	Collecting and transferring regolith
Total Battery	480 Wh	Sufficient power for multiple trips per day

STiM Power Budget		
Mode	**Power Draw**	**Description**
Sintering	4 kW	3 1.5 kW RF generators, press, and controls
Ejecting Tiles	0.40 kW	Moving finished bricks off the STiM
Conditioning	250 W	Vibratory screening and release actuation
Idle (Day)	50 W	Electronics on standby, ready for next cycle
Idle (Night)	<10 W	Survival heating, comms only

C. Cost Estimate

Table 12 Cost budget summary for the rover and STiM systems.

Rover Cost Budget		STiM Cost Budget	
Category	**Cost (USD)**	**Category**	**Cost (USD)**
Power & Thermal	570,000	Structure & Mechanical Systems	3,625,000
Navigation Sensors (IMU + Cameras)	1,250,000	Electronics & Avionics	1,150,000
Structure & Mechanical Systems	3,650,000	Actuation (Motor & Gearboxes)	845,000
Electronics & Avionics	1,030,000	Regolith Processing (Microwave & Mold)	2,753,500
Actuation (Motor & Gearboxes)	780,000	Power & Thermal	1,392,000
Software & Integration	500,000	Software & Integration	1,500,000
Space-Safe Modifications (600%)	46,680,000	Space-Safe Modifications (600%)	187,750,000
Total Cost	**54,460,000**	**Total Cost**	**196,537,500**
		System Total Cost	**250,997,500**

VII. Discussion

The final design shows that autonomous lunar landing pad construction using ISRU is feasible within the constraints of the Griffin lander payload. Throughout the design process, the two largest drivers were mass and available power. These constraints shaped nearly every major decision, including the selection of a hybrid architecture with a lightweight regolith collection rover and a stationary tile manufacturing unit. This approach allows the rover to remain small and mobile while placing the most power-intensive processes at the lander, where power access is greatest.

The fabrication trade study also supports this final configuration. Binder-based methods were ruled out because they require Earth-delivered consumables, which would reduce scalability and consume too much of the mass budget. Solar sintering had advantages in simplicity of energy source, but it was limited by dependence on illumination and reduced control over the heating process. Microwave sintering was therefore selected because it provides better control, can operate independent of direct sunlight, and is more compatible with the overall architecture of the system.

The landing site and regolith analysis further support the feasibility of the concept. The Mons Mouton Plateau, specifically the Nobile Rim 1 region, provides a strong balance between illumination, terrain safety, communications access, and regolith suitability. In addition, the regolith analysis showed that particle size, composition, and thermal behavior are all critical to tile performance. Fine regolith with strong microwave absorption characteristics is especially important for reducing porosity and producing stronger sintered tiles.

The system-level analysis also shows that the selected design remains within the project limits. The rover mass remains below its allocated 30 kg budget, and the total system mass remains below the 200 kg mission limit. This is important because it shows that the concept is not only functionally possible, but also realistic within the delivery constraints of the mission. The tile design and sintering approach also indicate that the produced tiles can satisfy the required loading conditions used in this project.

At the same time, there are still important limitations. The sintering model relies on available material-property data and simplifying assumptions, and the actual behavior of lunar regolith may vary depending on local composition and operating conditions. Similarly, although the tile design meets the required loading conditions in the current analysis, the system would still benefit from additional testing and validation using representative regolith simulants. Future work should focus on improving the sintering model, validating the thermal and structural performance of the tiles, and demonstrating repeated end-to-end rover and tile maker operations.

VIII. Conclusion

This work presents a conceptual mission for autonomous construction of lunar landing pad infrastructure using in-situ resource utilization and microwave sintering. The resulting design combines a mobile regolith collection rover with a stationary tile manufacturing unit, allowing the system to use local lunar material while remaining within the strict mass and power constraints of the Griffin lander.

The final concept demonstrates that a payload of this type can remain below the 200 kg mission mass limit while still supporting excavation, conditioning, microwave sintering, cooling, and tile deployment. Microwave sintering was selected as the preferred fabrication method because it offers the best balance of controllability, independence from consumable materials, and scalability for long-duration lunar construction. The selected landing site at Mons Mouton Plateau further supports the mission by providing favorable illumination, accessible terrain, and suitable regolith conditions.

Overall, the VT LUNA concept shows that autonomous tile-based landing pad construction is a realistic first step toward broader lunar surface infrastructure. By reducing plume ejecta risk and enabling incremental expansion of hardened landing areas, this system could support safer and more sustainable lunar operations as Artemis missions move toward a permanent surface presence.

Acknowledgments

The authors thank Dr. Kevin Shinpaugh of the Virginia Tech Kevin T. Crofton Department of Aerospace and Ocean Engineering for his guidance throughout this project, and the Consortium for Space Mobility and ISAM Capabilities (COSMIC) for organizing the C3 Capstone Challenge.

References

[1] NASA, "Lander Plume Ejecta — Experimental and Numerical Results," Technical Report NASA / TM-2020-503590, NASA, 2020. URL https://ntrs.nasa.gov/api/citations/20205003590/downloads/20_Wittaletal_LanderPlumeEjecta.pdf, accessed 2025-12-10.

[2] "C3 — CosmicSpace.org," , ???? URL https://cosmicspace.org/c3/, accessed 2025-12-10.

[3] "Astrobotic.com," , ???? URL https://www.astrobotic.com/lunar-delivery/landers/griffin-lander/, homepage, accessed 2025-12-10.

[4] Giwa, I., et al., "3D Printed Sulfur-Regolith Concrete Performance Evaluation," *Construction and Building Materials*, 2024. URL https://www.sciencedirect.com/science/article/abs/pii/S0926580524003078, study on sulfur binder concrete for lunar construction.

[5] Lim, S., et al., "Investigating the microwave heating behaviour of lunar soil," *Scientific Reports*, Vol. 11, 2021, pp. 1–12. URL https://www.nature.com/articles/s41598-021-81691-w, shows microwave heating as more viable than solar sintering for regolith processing.

[6] Bryant, S., "Lunar Pole Illumination and Communications Maps Computed from Goldstone Solar System Radar Elevation Data," Interplanetary Network Progress Report 42–176, Jet Propulsion Laboratory, California Institute of Technology, February 2009. URL https://ipnpr.jpl.nasa.gov/progress_report/42-176/176C.pdf, accessed 2025-12-10.

[7] "NASA Identifies Candidate Regions for Landing Next Americans on the Moon," , 2024. URL https://www.nasa.gov/news-release/nasa-identifies-candidate-regions-for-landing-next-americans-on-moon/, accessed 2025-12-10.

[8] "NASA Provides Update on Artemis III Moon Landing Regions," , 2022. URL https://www.nasa.gov/news-release/nasa-provides-update-on-artemis-iii-moon-landing-regions/, accessed 2025-12-10.

[9] European Space Agency, "Microwave Heating of Lunar Regolith (Microlith)," https://www.youtube.com/watch?v=4WguxZl0O-U, 2025. YouTube video, accessed 12 December 2025.

[10] Strangway, W., D. Pearce, W., G. and Olhoeft, R., G. "Magnetic and Dielectric Properties of Lunar Samples," *Proceedings of the Soviet–American Conference on Cosmochemistry of the Moon and Planets, Part 1*, NASA, Washington, DC, 1977. URL https://ntrs.nasa.gov/citations/19780005009, nASA Technical Reports Server (NTRS) Document ID: 19780005009.

[11] Lee, H., Jun, S., Kim, J., Kim, D., Lee, S., and Park, J., "Microwave Sintering of Lunar Soil Simulant for In-Situ Resource Utilization," *Scientific Reports*, Vol. 11, 2021, p. 791. https://doi.org/10.1038/s41598-021-81691-w, URL https://www.nature.com/articles/s41598-021-81691-w, accessed 12 December 2025.

[12] of the paper, A., "Title of the Article," *Scientific Reports*, Vol. 14, 2024, p. 79504. https://doi.org/10.1038/s41598-024-79504-x, URL https://www.nature.com/articles/s41598-024-79504-x, accessed 12 December 2025.

[13] Warren, P., Raju, N., Ebrahimi, H., Krsmanovic, M., Raghavan, S., Kapat, J., and Ghosh, R., "Effect of Sintering Temperature on Microstructure and Mechanical Properties of Molded Martian and Lunar Regolith," *Ceramics International*, Vol. 48, No. 23, 2022, pp. 35825–35833. https://doi.org/10.1016/j.ceramint.2022.07.329.

[14] Air Force Flight Dynamics Laboratory, "Analysis of Plates in Bending," https://engineeringlibrary.org/reference/analysis-of-plates-bending-air-force-stress-manual, 1986. Chapter from the Stress Analysis Manual.

[15] Pastore, A., Agozzino, M., and Ferro, C. G., "A Lunar Landing Pad from IRSU Materials: Design and Validation of a Structural Element," *Aerospace*, Vol. 12, No. 9, 2025, p. 781. https://doi.org/10.3390/aerospace12090781, URL https://www.mdpi.com/2226-4310/12/9/781.

[16] Watson-Morgan, L., Hawkins, L., Crisler, J., Gagliano, L., Ortega, R., Percy, T. K., Polsgrove, T., and Vermette, J., "NASA's Initial Artemis Human Landing System," *73rd International Astronautical Congress (IAC)*, International Astronautical Federation (IAF), Paris, France, 2022. URL https://ntrs.nasa.gov/api/citations/20220013431/downloads/HLS%20IAC_Final.pdf, document ID 20220013431, available from NASA Technical Reports Server.

[17] Jehn, I. E., and Dreyer, C. B., "A design methodology for flat slab lunar landing and launch pad systems," *Acta Astronautica*, Vol. 231, 2025, pp. 175–192. https://doi.org/10.1015.

[18] Indyk, S. J., et al., "A structural assessment of unrefined sintered lunar regolith," *Acta Astronautica*, Vol. 139, 2017, pp. 353–362. https://doi.org/10.1016/j.actaastro.2017.03.012.

[19] Kim, Y.-J., Ryu, B.-H., Jin, H., Lee, J., and Shin, H.-S., "Microstructural, mechanical, and thermal properties of microwave-sintered KLS-1 lunar regolith simulant," *Ceramics International*, Vol. 47, No. 19, 2021, pp. 26891–26897. https://doi.org/10.1016/j.ceramint.2021.06.098, URL https://www.sciencedirect.com/science/article/pii/S0272884221018423.

[20] Farries, K. W., Visintin, P., Smith, S. T., and van Eyk, P., "Sintered or melted regolith for lunar construction: state-of-the-art review and future research directions," *Construction and Building Materials*, Vol. 296, 2021, p. 123627. https://doi.org/10.1016/j.conbuildmat.2021.123627.

[21] Han, W., Zhou, Y., Cai, L., Zhou, C., and Ding, L., "Physical, Mechanical and Thermal Properties of Vacuum Sintered HUST-1 Lunar Regolith Simulant," *International Journal of Mining Science and Technology*, Vol. 34, 2024, pp. 1243–1257. https://doi.org/10.1016/j.ijmst.2024.06.004, URL https://www.sciencedirect.com/science/article/pii/S2095268624000764.

[22] Taylor, L. A., and Meek, T. T., "Microwave Sintering of Lunar Soil: Properties, Theory, and Practice," *Journal of Aerospace Engineering*, Vol. 18, No. 3, 2005, pp. 188–196. https://doi.org/10.1061/(ASCE)0893-1321(2005)18:3(188), URL https://ascelibrary.org/doi/abs/10.1061/(ASCE)0893-1321(2005)18:3(188).

[23] Olhoeft, G. R., "Lunar Sample Electrical Properties," *Lunar and Planetary Science Conference Proceedings*, 1973. URL https://articles.adsabs.harvard.edu/full/1973LPSC....4.3133O/0003133.000.html, presented at the 1973 Lunar and Planetary Science Conference.

[24] Alibaba Group, "Alibaba.com: Global Wholesale Marketplace," , 2026. URL https://www.alibaba.com/, accessed: 2026-04-09.

[25] Miranda, F. A., Nessel, J. A., Romanofsky, R. R., and Acosta, R. J., "A Review of Antenna Technologies for Future NASA Exploration Missions," Tech. rep., NASA Glenn Research Center, 2006.

[26] Astrobotic Technology, Inc., "Astrobotic Lunar Landers: Payload User's Guide," Tech. Rep. Version 5.02, Astrobotic Technology, 2021.

[27] Silicon Laboratories, "WGM160P Wi-Fi® Module Data Sheet," , 2025.

[28] European Space Agency, "Communicating from Space: Gaining a Grip on Antennas," European Space Agency, 2025.

[29] Dunmore Aerospace, "Aluminized Kapton® Film & Aluminized Polyimide Film," https://www.dunmore.com/products/aluminized-polyimide-film.html, 2025.

[30] Finckenor, M. M., and Dooling, D., "Multilayer Insulation Material Guidelines," NASA Technical Publication NASA/TP-1999-209263, NASA Marshall Space Flight Center, 1999.

[31] NASA Glenn Research Center, "Aerogel Reinforced Composites (LEW-TOPS-141)," https://technology.nasa.gov/patent/LEW-TOPS-141, n.d.

[32] Thermtest, Inc., "A Brief Overview of Multilayered Insulation and Its Role in Protecting Spaceships and for the Extreme Temperatures in Space," https://thermtest.com/a-brief-overview-of-multilayered-insulation-and-its-role-in-protecting-spaceships-and-for-the-extreme-temperatures-in-space, Feb 2022.

[33] Kleinhans, M. G., et al., "Vacuum Effects on Lunar Soil Simulants: Implications for Trafficability and Construction," *Planetary and Space Science*, Vol. 210, 2025, p. 105467. https://doi.org/10.1016/j.pss.2025.105467, URL https://www.sciencedirect.com/science/article/pii/S0094576525007660, accessed 2025-12-12.

[34] Qian, C., et al., "The Influence of the Particle Size Distribution on SL-Manufactured Alumina Ceramics," *Ceramics International*, Vol. 48, No. 15, 2022, pp. 2022–2036. https://doi.org/10.1016/j.ceramint.2022.07.123, URL https://www.sciencedirect.com/science/article/pii/S0272884222012950, accessed 2025-12-10.

[35] IntoCeramics, "Ceramic Materials & The Role of Powder Particle Size," , 2024. URL https://www.intoceramics.com/blog/ceramic-materials-powder-particle-size, blog post, accessed 2025-12-10.

[36] Tachikawa, S., Nagano, H., and Ohnishi, A., "Advanced Passive Thermal Control Materials and Devices for Spacecraft: A Review," *International Journal of Thermophysics*, Vol. 43, No. 91, 2022.

[37] National Aeronautics and Space Administration (NASA), "Radioisotope Heater Unit (RHU) Fact Sheet," Tech. rep., Department of Energy, 2020. URL https://rps.nasa.gov/power-and-thermal-systems/thermal-systems/light-weight-radioisotope-heater-unit/.

[38] Allan, S. M., Merber, B. J., et al., "High-Temperature Microwave Dielectric Properties and Processing of JSC-1AC Lunar Simulant," *Journal of Aerospace Engineering*, Vol. 26, No. 4, 2013, pp. 874–881.

[39] Gilmore, D. G., *Spacecraft Thermal Control Handbook*, Vol. 1, The Aerospace Press, El Segundo, CA, 2002.

[40] Peng, F., Jiang, Y., et al., "Thermally Insulating, Fiber-Reinforced Alumina–Silica Aerogel Composites with Ultra-Low Shrinkage up to 1500 °C," *Chemical Engineering Journal*, Vol. 411, 2021, p. 128402.

[41] Uyanna, O., and Najafi, H., "Thermal Protection Systems for Space Vehicles: A Review on Technology Development, Current Challenges and Future Prospects," *Acta Astronautica*, Vol. 176, 2020, pp. 341–356.

[42] Microchip Technology, "SAMRH71 Radiation-Hardened Microcontroller," , 2026. URL https://www.microchip.com/en-us/product/samrh71, accessed: 2026-04-09.

[43] Microchip Technology, "LX7720 Motor Controller," , 2026. Accessed: 2026-04-09.

[44] Northrop Grumman, "LN-200S Inertial Measurement Unit," , 2026. URL https://www.northropgrumman.com/what-we-do/mission-solutions/assured-navigation/ln-200s-inertial-measurement-unit, accessed: 2026-04-09.

[45] Minco Products, Inc., "Polyimide (Kapton) Etched-Foil Heaters," , 2026. URL https://www.minco.com/products/thermal-solutions/heaters/polyimide-heaters/, typical specs: thickness ~0.25 mm; customizable sizes (e.g., 75 × 75 mm); power range varies (commonly 5–10 W for small heaters); Accessed: 2026-04-09.